Radioactive Source Calibration Technique for the CMS Hadron Calorimeter

E. Hazen, C. Lawlor, J. Rohlf, and S. X. Wu

Boston University, Boston, MA 02212

A. Baumbaugh, J. E. Elias, J. Freeman, D. Green, D. Lazic, S. Los, A. Ronzhin, S. Sergueev, T. Shaw, R. Vidal, J. Whitmore, and T. Zimmerman

Fermi National Accelerator Laboratory, Batavia, IL 60510

M. Adams, K. Burchesky, and W. Qian

University of Illinois, Chicago, IL

A. Baden, R. Bard, H. Breden, T. Grassi, and A. Skuja

University of Maryland, College Park, MD 20742

W. Fisher, J. Mans, and C. Tully

Princeton University, Princeton, NJ 08540

V. Barnes and A. Laasanen

Purdue University, West Lafayette, IN 47907

P. de Barbaro and H. Budd

University of Rochester, Rochester, NY 14627

Preprint submitted to Elsevier Science *15 February 2003*

Abstract

Relative calibration of the scintillator tiles used in the hadronic calorimeter for the Compact Muon Solenoid (CMS) detector at the CERN Large Hadron Collider (LHC) is established and maintained using a radioactive source technique. A movable source can be positioned remotely to illuminate each scintillator tile individually, and the resulting photo-detector current is measured to provide the relative calibration. The unique measurement technique described here makes use of the normal high-speed data acquisition system required for signal digitization at the 40 MHz collider frequency. The data paths for collider measurements and source measurements are then identical, and systematic uncertainties associated with having different signal paths are avoided. In this high-speed mode, the source signal is observed as a Poisson photo-electron distribution with a mean that is smaller than the width of the electronics noise (pedestal) distribution. We report demonstration of the technique using prototype electronics for the complete readout chain and show the typical response observed with a 144 channel test beam system. The electronics noise has a root-mean-square (r.m.s.) of 1.6 least counts, and a 1-mCi source produces a shift of the mean value of 0.1 least counts. Because of the speed of the data acquisition system, this shift can be measured to a statistical precision better than a fraction of a percent on a millisecond time scale. The result is reproducible to better than 2% over a time scale of one month.

Keywords: Hadron Sampling Calorimeter, Radioactive Source Calibration

PACS Numbers: 29.40.Mc, 29.40.Vj, 29.90.+r

Please send proofs to:
James W. Rohlf
Department of Physics
590 Commonwealth Avenue
Boston University
Boston, MA 02215
tel.: 617-353-6035, fax.: 617-353-9393, email: rohlf@bu.edu

1 Introduction

The CMS detector [1] is designed to study proton-proton collisions at a center-of-mass energy of 14 TeV and luminosity of 10^{34} cm^{-2}s^{-1} at the LHC presently under construction at CERN. The detector design follows conventional practice for full solid angle coverage and includes a central precision tracking detector, separate electron and hadron calorimeters in a central-barrel and end-cap cylindrical configuration, and a high-field solenoidal superconducting coil all surrounded by layers of iron absorber and muon tracking chambers. A unique feature of the design is the size of the coil; all of the calorimetry as well as the tracker reside inside the 4-tesla field volume.

The hadron calorimeter [2] (HCAL) is a sampling detector constructed of brass (non-magnetic) absorber plates and plastic scintillator sampling layers. Detailed results from a prototype device and optimization of the final choice of absorber depth, sampling frequency and longitudinal segmentation can be found in Ref. [3]. Scintillator layers are segmented into individual tiles (approximately 20 cm by 20 cm) sized to form projective towers that point back to the interaction point. Light from each scintillator tile is wavelength shifted and extracted via plastic fibers doped with a fluorescent dye embedded in grooves in the tiles. Clear plastic fibers are used to pipe the shifted light to the back surface of the calorimeter where the photo-detectors and front-end electronics are located. By grouping the clear fibers from each layer appropriately, bundles are formed that correspond to the projective towers, and these bundles are each attached to a photo-detector.

1.1 Choice of Photo-Detector

A complex set of requirements and constraints severely limit the choice of photo-detector. Operation in the 4-tesla field, exposure to a neutron flux of 2×10^{11} cm^{-2} during ten years of operation, adequate signal-to-noise for muon detection and efficient use of photo-detector surface area are the most demanding of these.

In the case of CMS, the nearest placement of phototubes outside the 4 Tesla magnet would be at a distance of 10 meters of clear fiber. At this location the stray field is 2 Tesla which means that multi-anode phototubes are not suitable. We considered single anode phototubes. Assuming that an operating phototube could even be developed, a major factor against using phototubes was the required volume inside the detector. Placement of 9000 tubes inside the detector would require about 150 cubic feet of volume, which was not available. In contrast, the volume required for the same number of channels using photo-

diodes is 5 cubic feet. To get the signals outside the magnet would require an additional 2400 km of clear fiber which would substantially compromise the hermeticity of the detector and would be substantially more expensive.

Following extensive investigations, a proximity-focused hybrid photo-diode [4] was selected as the photo-detector. Because these devices operate at low gain, typically 2000, special requirements are placed on the calibration system.

1.2 Activation of the Detector

During the lifetime of the CMS experiment, the absorber will become activated. Extensive Monte Carlo studies indicate that the worst-case dose in the central hadron calorimeter is at the high eta corner of the endcap calorimeter. After a run of 60 days at full luminosity and a cool-down period of one day (a condition under which we may make a radioactive source calibration), we estimate that the dose-rate in this location will be 330 mSv/hr. Since this is a bulk activation, many of the scintillator tiles in this tower will experience roughly the same dose-rate. This activation will generate a DC-level of additional current that will be present during the source run. Our calculations indicate that this additional current will be at a level of about 5% of that generated by the radioactive source. We believe that this will present no problem to our ability to perform accurate source calibrations. We note that the ZEUS uranium calorimeter also uses a moving radioactive source for calibration. There, the deleted uranium absorber presents a continual background current. In the case of ZEUS the background current is larger than that created by the radioactive source [5]. In their case as well as ours, however, the background current simply appears as a pedestal shift in the measurement and does not affect the accuracy of the calibration.

1.3 Technique for Measuring Source Signal

Radioactive source techniques have been very successful in establishing relative calibrations for scintillators and in tracking their response in time as systems age or suffer radiation damage. The challenge in applying this technique to the CMS hadron calorimeter follows from the low gain of the photo-detector. One possible approach, use of special circuitry that is switched in only for source measurements, adds both complexity and additional failure risk and introduces a systematic uncertainty due to the necessary cross-calibration with the normal signal path. The unique measurement technique adopted was to use the existing high-speed signal processing system without change. Thus, issues of cross calibration and systematic bias are avoided, while issues of noise level, noise stability and linearity become of paramount importance.

When sampled at the 40 MHz collider frequency, the signal from the source illuminating a single scintillator tile is a Poisson photo-electron distribution, not a direct current. The difference in response between the source on and source off condition is only a fraction of a least significant bit in the high-speed, flash analog-to-digital-converter (FADC). The excellent differential nonlinearity of this custom FADC in the fast signal data acquisition path allows for a precise measurement of the small shift, given that the r.m.s of the noise (pedestal) distribution is about 1.6 least counts and the distribution spans a number of bins. The high statistics provided by the 40 MHz digitization and readout system leads to precise determinations of the mean value on a millisecond time scale, thus easing the noise stability requirement. The r.m.s. resolution achieved on the source signal (σ_{signal}) from taking the simple difference of the means, source on minus source off, and not the other shape information is given by

$$\sigma_{signal} = \frac{\sqrt{2}\sigma_{noise}}{\sqrt{N}}, \tag{1}$$

where σ_{noise} is the r.m.s. of the noise and N is the number of events. For $\sigma_{noise} = 1.6$ and $N = 10^6$, we get $\sigma_{signal} = 0.002$, giving a 2% measurement for a source which gives a mean signal of 0.1 least count. As will be shown, we can achieve this resolution with a much smaller data sample by fitting the measured source-on distribution to an unknown Poisson signal plus a known, independently measured Gaussian noise.

In the following, we describe the high-speed readout chain from the photo-detector to the in-crate processor in order to fully present the measurement technique. Data on noise characteristics are presented next followed by a demonstration of the technique first with an light emitting diode (LED) as the light source and then with the source/scintillator combination as in the actual calorimeter. Finally, we show an example of the excellent results obtained in a test-beam environment with a 144-channel system and the production calorimeter.

2 Conceptual Design of HCAL Calibration

Degradation of the calorimeter signals is expected to arise from radiation damage, scintillator aging, and changes in photo-detector response. The absolute calibration of the hadron calorimeter comes from response in a test beam and is carried over to the experiment with a moving radioactive source similar to that used in the Collider Detector Facility (CDF) experiment [6]. The principle difference between our calibration system and the CDF system is that

our low-gain photo-detectors produce a signal in response to the radioactive source which is much smaller than the electronics noise.

Each row of towers in the scintillator trays of the CMS calorimeter has a stainless steel tube that carries a radioactive source along its length. A schematic layout of the source tubes is shown in Fig. 1. Due to space limitations, sources are permanently attached to only two layers of the barrel, immediately after the electromagnetic calorimeter and the in the middle layer. In the end cap. several layers are permanently monitored because of the higher level of radiation damage. These layers can be monitored with moving sources, as needed, between physics runs, approximately once per month. Source calibration of all of the scintillators is possible only during an extended shutdown when the detector is open, approximately once per year.

The low gain of the hybrid photo-diodes in HCAL presents a challenge for the calibration: precision measurement of a small current ($\sim$5 nA) induced by the radioactive source in the presence of a comparable dark current. Nore that the growth in photo-detector dark-current in the radiation field expected at CMS does not adversely effect the detector calibration [2]. The technique chosen is to use the same high-speed, 80 MBytes/s data acquisition readout as used for colliding beams data. Pedestal distributions are simultaneously accumulated from those scintillators not being illuminated by the source. As the source traverses a given scintillator, there is a slight broadening and upward shift of the pedestal distribution. The calibration is clearly insensitive to possible shifts in the pedestal over timescales that are larger than the ms data collection time.

The source moves across a scintillator tray at 10 cm/s. With the front-end electronics clocked at the LHC machine frequency of 40 MHz, 800k events can be collected every 2-mm. This is a sufficient number of events to meet the goal of a 2% measurement of the source response in the absence of systematic errors. The time taken to scan back-and forth across the longest scintillator trays is about 90 s, corresponding to 3.6 Gb of data. As it is not practical or desirable to store all this raw data, firmware in the readout electronics will accumulate histograms at each 2 mm position. From these histograms, numerical values for the signals characterizing the source response will be extracted for each scintillator.

3 Apparatus

A block diagram of the apparatus used for the radioactive source measurements is shown in Fig. 2. The apparatus is a prototype version of that planned for HCAL readout at the LHC. For the measurements reported here, there

was a complete readout chain from scintillator to computer. The essential electronic elements were: hybrid photo-diode (HPD), charge integration and encoding (QIE), trigger and readout module (HTR), trigger timing and control system (TTCvi, TTCvx, and TTCrx modules) and data concentrator card (DCC). Three separate data links are used in the readout chain: an optical (G-LINK) from the front-end electronics to the readout card, a copper link (Channel Link) from the readout card to the data concentrator, and an optical (S-LINK) from the data concentrator to the computer.

3.1 Scintillator

The geometry of the scintillator used for the radioactive source measurements is shown in Fig. 3. The 2-cm thick plastic scintillator used for these measurements was of the same type (Bicron BC408) as that used in the first physical layer of the barrel calorimeter. The scintillation light was collected by several 0.83-mm diameter fibers (Kuraray multiclad). The scintillator was housed in a box which had a socket into which a radioactive source could be inserted.

3.2 Hybrid Photo-Diode

Each bundle of fibers corresponding to an η, ϕ tower of the barrel and end-cap calorimeters is coupled to a hybrid photo-diode (HPD) pixel [4]. The HPD is linear over a wide dynamic range and can operate in a high magnetic field when the field is aligned to the axis of the applied electric field. The HPD has a multi-alkali photo-cathode deposited on a fiber-optic entrance window. Following the photo-cathode is a gap of several millimeters where a large applied electric field accelerates photo-electrons which strike a silicon diode target, producing electron-hole pairs. For these tests, the high voltage was set at 7 kV, resulting in a gain of about 1700 which is a somewhat smaller gain than foreseen during CMS operations.

The silicon diode target is divided into 19 pixels as indicated in Fig. 4 so that a 20-degree region of the barrel or end-cap (72 channels) is read out with four HPDs. For these tests the fiber bundle from the scintillator was aligned with a single pixel in the HPD. The leakage current for this pixel was measured to be 4.6 nA. Also included in the system was a light-emitting diode (LED) which could be pulsed for diagnostic purposes.

3.3 Front end Electronics

Conditions at the LHC demand that the HCAL front-end electronics be low-noise (less than 3000 electrons), high-frequency (40 MHz) and digitize over a wide dynamic range (1/3 fC least count, 16 bit). In addition, there are special requirements on reliability, radiation tolerance, magnetic field immunity, cross talk, and capabilities for DC current measurement. A block diagram is shown in Fig. 5.

Analog signals are processed through a current splitter and gated integrators. The HCAL design is based on an improvement of the analog processing ASIC developed for the KTeV experiment at Fermilab [7]. This ASIC is referred to by its functions of charge integration and encode (QIE). The CMS version is referred to as QIE8. The signal is digitized in an 7-bit pseudo floating-point format with 2 bits of range (exponent) and 5 bits of mantissa. The QIE contains four sets (referred to as cap ID 0, 1, 2 and 3) of four integrators with weighted equivalent capacitance attached to a current splitter. Equal sharing of current in matched common-base transistors connected in parallel is used to apportion a fixed fraction of the input current to a given integrator in the array, with each integrator receiving a fraction of the current of its lower-range neighbor. A combination of the splitting ratios and integrator capacitances gives four ranges with relative sensitivities of 1:5:25:125 fC per least significant bit (LSB). The input current is simultaneously integrated on all ranges and comparators select the lowest range that is not full scale. The voltage on the integrator provides the mantissa, while its address provides the range. The operations are multiplexed and pipelined with a four-cycle latency. One set integrates the input current for one LHC bunch crossing interval (25 ns). The other three sets of integrators are settling, being read out, and being reset, respectively.

There are two input paths, one for the signal and one for a reference input. The cabling and circuitry is identical for both inputs, so that the technique results in common mode rejection of external noise and internal bias variations. They are combined together before being digitized in an integrated FADC. The input must settle to about 1/4 least count in one 25-ns clock interval, implying about 60 MHz bandwidth for components on the analog signal path.

For the radioactive source measurements, it is important that the ADC bin widths remain constant in the region near the pedestal. Special care has been taken in the QIE8 design to achieve a differential nonlinearity less than about 2% LSB.

Ancillary circuitry is shown in Fig. 6. Since the QIE is a synchronous, pipelined

device with multiple state machines, it is necessary at power up to place all QIEs in a known state within a precision of one clock cycle. The cap ID and range bits come directly from the range encoder and state machine while the mantissa is digitized by the FADC. A separate channel control ASIC transfers data to a high-speed optical link for transmission to the trigger and readout cards, and supplies the clock to the QIE. These bits are aligned inside the QIE8.

For the source calibration, there is a special mode in which the FADC bin width is changed by a factor of three, using just the lower end of the FADC for this mode, so that one least count is 1/3 fC. With an HPD gain of 1700, this corresponds to 1.2 photo-electrons per least count referred to the HPD cathode.

Due to a slower than expected rise time of the FADC comparator digital outputs, the prototype version of the QIE used for these measurements was not able to run at a clock frequency of 40 MHz. The electronics was therefore run at 35 MHz for the measurements described in this paper. The design has subsequently improved so that speeds of 60 MHz are possible.

3.4 Clock

A fundamental clock requirement in the final HCAL architecture is to strictly synchronize the Front-End with the HCAL trigger and readout module, as this module will generate the primitives for the trigger system. In view of this we used the trigger timing and control (TTC) system [10]-[11] developed at CERN for clock distribution at the LHC. The components used for these tests are the TTCvi, TTCvx, and TTCrx (see Fig. 2). The TTCvi [12] is a VME interface module that is designed to be phase-locked to the LHC bunch-crossing frequency of 40.079 MHz. For these measurements, the TTCvi was provided with a 35 MHz clock from a Hewlett Packard frequency generator. The TTCvx [13] is a low-power VME6u-sized LED transmitter module that delivers a common optical signal to up to 4 destinations, in this case, the front-end electronics and the HTR. The TTCrx [14] is a custom integrated circuit designed by the CERN EP Microelectronics Group which receives the clock together with control and synchronization information.

3.5 G-LINK

The prototype design used G-LINK [8] for point-to-point data transfer from the front-end electronics to the readout modules. Data from two channels were transmitted serially on a single optical link. The data were sent in 16-bit words

with the following format: channel-A mantissa (bits 0-4), channel-A exponent (bits 5-6), channel-B mantissa (bits 7-11), channel-B exponent (bits 12-13), and capacitor identity (bits 14-15). The data transfer rate was 70 MBytes per second for these measurements, the QIE clock frequency times 16 bits.

Correct data reception in the HCAL trigger and readout (HTR) module required an appropriate scheme for the three clocks involved: the TTC clock, the clock recovered from the incoming data and the clock from a local oscillator. For this particular application, the readout module was configured to use the recovered clock as a board system clock.

3.6 Trigger and Readout Module

The HTR module is designed to receive data on optical links, determine the energy for each tower, identify the bunch crossing and send these data to a regional calorimeter trigger module. If there is a trigger, the raw data are sent to a data concentrator module (DCC) on copper twisted-pair cable. The conceptual design of the HCAL readout is described in Ref. [9].

The prototype version of the HTR used for these measurements is a 4-channel unit whose main component is an Altera APEX EP20k400BC652-1V. A block diagram is shown in Fig. 7. The prototype HTR could run in three different modes, selectable by a front panel switch. A repetitive mode sends data from an internal 16-bit counter to the DCC in order to test the HTR to DCC communication, independent of the HTR input. A data stream mode sends the 16-bit input received over G-LINK on to the DCC without alteration so that the link could be tested with minimum firmware running in the HTR.

Finally, a source mode, which was used for these measurements, rearranges the bits of the QIE data to accommodate G-LINK and cap ID error bits. In order to fit two channels in a single 16-bit word, the range bits, which are not used for the source calibration, are combined for the two channels (logical "or"). The data format is channel-A mantissa (bits 0-4), channel-A or channel-B exponent (bits 5-6), channel-B mantissa (bits 7-11), G-LINK error (bit 12), cap ID error (bit 13) and cap ID (bits 14-15). In this mode, since the source is not triggerable, the HTR generates an internal periodic signal that emulates the trigger input. This signal is necessary to create the output data format for the communication with DCC, as this data format is based on single events. The format introduces less than 1.2% dead-time, negligible for the purpose of the source calibration.

3.7 Channel Link

The data path from the HTR to the DCC uses low voltage differential signaling (LVDS) implemented with National Semiconductor's Channel Link technology [15]. Each link receiver (Fig. 8) can receive 16-bit words at up to 66MHz. The data transfer rate over the Channel Link was 70 MBytes per second for these measurements.

Each link has buffering for 128k 32-bit words, with provision to discard data if the buffer occupancy exceeds a programmable threshold. The link receivers were built on daughter boards that each contain three independent Channel Links. A personal computer interface (PCI) target interface provides single-word and burst access to the data stream, plus numerous monitoring registers. A single PCI burst read transfers the next data block to the PCI master.

Hamming error correction is used for the LVDS links between the HTR and DCC. All single-bit errors are corrected and all double-bit errors are detected by this technique. The link receiver writes a link-error byte and word count into the trailer. The possible error conditions are: corrected link error, uncorrected link error, block size overflow, block number header/trailer mismatch, FIFO empty with no trailer seen, FIFO overflow, block structure error, and odd 16-bit word count. The data are transferred over the PCI bus as 32-bit words.

A link transmitter card was available to send a known data pattern to the link receivers, which proved extremely useful for independent debugging of the Channel Link. The transmitter card may be mounted on the DCC motherboard and is interchangeable with any of the link receiver cards. This gave the DCC the capability of transmitting to itself, allowing debugging as a standalone system.

3.8 Data Concentrator Card

The data concentrator card (DCC) [9] is designed to receive data from up to 18 HTR boards, assemble the event, and provide outputs to the data acquisition, fast monitor, trigger spy, and event spy.

The DCC is built on a VME64x 9Ux400mm motherboard, which can accommodate up to six 3-channel LVDS link receiver boards and a PCI mezzanine card (PMC) logic board. The motherboard (Fig. 9) supports VME access up to A64/D32, and contains three bridged PCI busses. Six PC-MIP mezzanine sites are arranged in groups of three on two 33MHz 32-bit PCI busses. A third 33MHz 64-bit PCI bus is bridged to the VME bus using a Tundra Universe

II VME-to-PCI bridge. A single large mezzanine board has access to all three PCI busses for high-speed application-specific processing, and an additional standard PMC site is available. A local control FPGA on the motherboard provides access to on-board flash configuration memory and a programmable multi-frequency clock generator.

The mezzanine board executes the core data concentrator algorithm. The prototype was implemented using a Xilinx XC2V1000 for the event assembler, plus three Altera EP1K30 for the three PCI bus interfaces.

For these measurements, the DCC operated in a simple "streaming" mode, where data was received by the DCC on a single link receiver board. Block reads were performed by the PCI bus 1 master interface from the link receiver, buffered in a FIFO, and transmitted via S-LINK to an in-crate CPU. As an alternate path for diagnostics, data can be written and read from the DCC's link receivers and logic card over VME.

3.9 S-LINK

In CMS, data will be transmitted from the DCC to the data acquisition stream via optical links based on S-LINK [16], a CERN specification for an easy-to-use FIFO-like data-link. S-LINK cards, PCI/PMC interfaces and test tools are all commercially available. The maximum transmission rate is 160 MBytes per second [17]. For these measurements, data were transmitted in 32-bit words from the DCC to the computer via S-LINK.

4 Software

4.1 Data Concentrator

A substantial software package has been developed to control and debug the DCC together with its link receivers and logic card. The package includes routines to initialize the DCC as well as to communicate with the link receivers and the logic card.

The software package is implemented in C++, and supports configuration and management of devices on multiple motherboards with 3 PCI busses on each. At initialization, all PCI devices in the system are configured, and a data structure is built which describes the hardware configuration. Known devices (link receivers, logic boards) have dedicated device drivers in the package, and

device-specific initialization is performed automatically. Unknown devices are configured generically according to the PCI bus specification and may also be used.

A simple interactive shell provides command-line access to all PCI devices on the motherboards. Initial debugging and operation of the DCC was performed using scripts written for this shell. A dedicated C program was used to control the DCC during the source test.

4.2 VME Interface Library

The DCC software makes use of a custom VME interface library (VMEIL) based upon a set of standard drivers for the Universe II [18]. The VMEIL is a linkable library which provides an interface between the VME-PCI Bridge driver and specific VME hardware drivers [19]. The VMEIL architecture gives a layer of abstraction between the VMEbus adapter and the VME hardware drivers, providing a convenient environment for debugging and code development.

4.3 Data Acquisition

Without a trigger system, the data acquisition was implemented in two steps. First, the S-LINK receiver was reset and the CPU was placed in a ready state for direct memory access (DMA). Second, the DCC was initialized and instructed to transmit any incoming data over S-LINK to the CPU. The software to control the DMA via S-LINK was based on a driver developed for the Canada-France-Hawaii Telescope [20]. The software allows fast transfer without user intervention to reserved, physically linear random access memory. The memory may be reserved without need of patching the kernel. A library is available for control of the S-LINK.

An interface displays useful statistics on the data transfered. For our application, the 448 MBytes of memory allocated to DMA allowed a 6.6-second continuous stream of data to be recorded. The G-LINK, LVDS Channel Link, and the S-LINK all repeatedly transmitted and received data along the entire readout chain without error. The data received from the DCC via S-LINK was augmented with a fixed header containing the run number and word count and a variable length trailer containing a time stamp and user comments before being written to disk. Approximately 30 GBytes of data were recorded for the measurements described in this paper.

5 Results

5.1 Pedestal Distributions

Figure 10 shows the pedestal distributions from each of the four cap IDs in the QIE for 100k events. Data from each cap ID is fit well with a Gaussian distribution with standard deviation of 1.3 least-significant-bit counts (LC), corresponding to a r.m.s. noise of slightly less than 2800 electrons.

The mean pedestal for each of the four cap IDs is not perfectly matched (see Table 1). The addition of these four Gaussian distributions results in a distribution (Figure 11) that is also nearly Gaussian with a width of 1.6, corresponding to about 3300 electrons, wider due to the different means of the capacitor pedestals.

Table 1
Measured front-end electronics noise.

Channel	*Pedestal (LSB)*	*RMS (LSB)*	*RMS (e)*
Cap ID 0	19.05	1.32	2750
Cap ID 1	18.31	1.32	2750
Cap ID 2	19.72	1.32	2750
Cap ID 3	17.28	1.34	2790
All (summed)	18.59	1.60	3330

5.2 Source Signal

A 0.98-mC Cs^{137} radioactive source was used for these measurements. Although this source was several times weaker than the source planned for CMS, it nevertheless was the strongest source allowed in the laboratory where these measurements were made. This source strength causes about one photon, on the average, to reach the HPD during one clock cycle. For a quantum efficiency of 12%, and 1.2 photo-electrons per least count in calibration mode for an HPD gain of 1700, we expect a signal of about 0.1 least counts from the radioactive source, per time sample. Thus, we are looking for a Poisson distribution with an approximate mean of 0.1 counts on top of a Gaussian noise distribution with a r.m.s. of 1.6 counts.

In order to observe the effect of the radioactive source, it was repeatedly

inserted and removed. Figure 12 shows a plot of the mean pedestal and source signal vs. time over a two hour period. Note that the vertical scale has a suppressed zero. In this plot, data from all four cap IDs are averaged together. Over this time period, a drift in the pedestal of the same order-of-magnitude as the source signal was observed. This drift was attributed to temperature effects as the HPD and front-end electronics were covered with several layers of black cloth for light shielding, and the entire apparatus was located in a small, enclosed room.

5.3 LED Signal

In order to make a precision measurement, pedestal and signal data were collected in the same DMA stream. The technique is illustrated in Fig. 13, where an LED was turned on and off during data collection. Each point in Fig. 13 is about 0.5 M events collected in about 14 ms. The rise time is about 14 ms for the LED response. Note the monotonic increase in light output over the 2.5 seconds that current was supplied as the device warmed up, and the immediate drop (14 ms fall time) to the original level when the LED is switched off.

5.4 Source and Mean Pedestal Shift

To make a signal measurement with the radioactive source, data collection was started with the source inserted and then it was extracted swiftly by hand during the 6.6 seconds of the DMA. Figure 14 shows one such DMA stream. The data have the same binning as that shown in Fig. 13. This plot shows a clear transition when the source is extracted. This allows many individual high-statistics measurements of the source signal and many such measurements of the pedestal immediately after removing the source. The distribution of these means for source in and source out are shown in Fig. 15a). Fig. 15b) shows the distribution of widths, further demonstrating the expected broadening of the Gaussian noise in the presence of the small Poisson source signal.

An identical change in signal strength was observed when the source was inserted during the DMA, instead of extracted, except that the rise time for insertion of the source by hand was a few tenths of a millisecond (compared to less than 0.1 ms for source extraction).

To further investigate the behavior of the QIE, the clock frequency was lowered from 35 MHz to 30 MHz. Data were collected as before with the source

being extracted during the DMA. With the increased integration time, there was a proprtional increase in the source signal to a value of 0.1022 ± 0.0002 LSB. Scaling the 35 MHz result of 0.0862 ± 0.0005 LSB by the inverse ratio of the clock frequencies (35/30), we predict a signal of 0.101 ± 0.001 LSB for the source signal at 30 MHz, in agreement with the measurement.

5.5 Poisson Source Signal

We have investigated the shape of the radioactive source signal. Figure 16 shows the pedestal distribution for all cap IDs (source out), while Fig. 16b) shows the observed distribution with the source inserted. The pedestal distributions from the four individual cap IDs were fitted to separate Gaussians with high statistics. The solid curve in Fig. 16a) is the sum of those four fits. The distribution with the source in has a higher mean (by 0.085 ± 0.002 counts) than with the source out, and also a slightly greater width (by about 0.08 channels).

Careful examination of Fig. 16 shows that the effect of the source is clearly visible. For example, with the source out channel 19 has 2600 more counts than channel 20, while with the source in channel 19 has 1000 fewer counts than channel 20 reflecting how the Poisson distribution from the source modulates the noise. The Poisson fit shown in Fig. 16b) gives a great improvement in statistical error over taking the straight difference of means (0.085 ± 0.002), and gives a signal of 0.0874 ± 0.0002 counts.

5.6 Source Signal and HPD Gain

To further investigate the small observed signal from the radioactive source, the HPD voltage was varied from 0 V to 9 kV, in 1-kV steps, corresponding to gains from zero to 2300. For each voltage, two separate short runs, source in and source out, were taken and the means of the two distributions were subtracted to get the source signal. These data, shown in Fig. 17, indicate that the response to the source is linear in high voltage as expected. Note that at low voltage, the thin inactive layer of diode electrode is evident in that there is an intercept of zero signal at about 1 kV.

5.7 QIE Nonlinearity

The differential nonlinearity of the QIE was investigated by varying the pedestal using programmable logic implemented on the QIE card to vary the standing input current. For each pedestal setting, the radioactive source was extracted during the data stream to get an accurate measurement of the source signal. In Fig. 18, we plot the percent deviation from the average source signal as a function of the pedestal value. The data do not deviate from channel to channel by more than one percent of the source signal, or 0.0008 least counts.

5.8 Long-Term Source Signal Stability

Figure 19 shows a summary of radioactive source measurements made on four different days spread over a one month period (January - February 2002). The measurements agree to slightly better than 2%. The small variation observed over the one-month period was likely dominated by mechanical alignment of the optical fibers with the appropriate HPD pixel, as much smaller variations ($< 1\%$) were observed over the time-scale of several hours when mechanical disturbance of the apparatus was kept to a minimum.

5.9 Test-Beam Environment

During the period July to September 2002, we made a calibration of four barrel wedges, comprising 4086 tiles of the production calorimeter, under the realistic conditions present in a testbeam at CERN. Analysis of the data taken will be the subject of subsequent publications. Systematic effects associated with variations of scintillator thickness, collimation of the radiactive source, and the presence of WLS in the final detector have been determined to be negligible. A better than 2% absolute calibration of these wedges was achieved using the technique described in this paper. The result of one such source scan is shown in Fig. 20. A continuous pedestal is measured before and after the moving source passes over the scintillator. The responce of the source is measured every centimeter to a precision of better than 1%. A fit to the data gives a source signal of 0.254 ± 0.001 least counts at the center of the tile.

6 Conclusion

The technique for calibration of the CMS hadronic calorimeter by a moving radioactive source, using only a single high-speed data path rather than a separate slow path for calibration has been demonstrated to be feasible using a source with an activity several times weaker than that planned for the experimental installation. This reduction to a single data path is made possible by fast data acquisition in which sufficient statistics are collected in less than 20 ms, so that a Poisson distribution of fractional photo-electron mean can be measured with better than 2% accuracy in the presence of a Gaussian noise of 1.6 photo-electrons (rms), with negligible systematic error.

7 Acknowledgments

We thank Erik van der Bij of CERN for his assistance with the S-LINK hardware and the grounding of the G-LINK transmitter chip. Sidik Isani of the Canada-France-Hawaii Telescope provided S-LINK to PCI driver software, and Guoan Hu of Boston University gave us his expertise on many items concerning the software. J. Rohlf acknowledges support from Fermilab which allowed a release from teaching duties.

8 Appendix

The following acronyms are used in this paper.

CDF: Collider Detector Facilility
CMS: Compact Muon Solenoid
DCC: Data Concentrator Card
FADC: Flash Analog-to-Digital Converter
FPGA: Field Programmable Gate Array
HCAL: Hadronic Calorimeter
HPD: Hybrid Photo-Diode
HTR: HCAL Trigger and Readout Module
LED: Light Emitting Diode
LHC: Large Hadron Collider
PCI: Personal Computer Interface
PMC: PCI Mezzanine Card
QIE: Charge Integration and Encoding
TTC: Trigger Timing and Control

References

[1] "CMS Technical Proposal," CERN/LHCC 94-38, LHCC/P1 (December 1994).

[2] "CMS, The Hadron Calorimeter Technical Design Report," CERN/LHCC 97-31 CMS TDR 2 (June 1997).

[3] V. V. Abramov *et al.* [CMS-HCAL Collaboration], "Studies of the Response of the Prototype CMS Hadron Calorimeter, Including Magnetic Field Effects, to Pion, Electron, and Muon Beams," Nucl. Instrum. Methods, A**457** (2001) 75.

[4] P. Cushman, A. Heering, and A. Ronzhin, "Custom HPD Readout for the CMS HCAL," Nucl. Instrum. Methods, A**442** (2000) 289.

[5] U. Behrens *et al.*, "Quality Control and Calibration of the ZEUS Forward and Rear Calorimters with Co-60 Sources," Nucl. Instrum. Methods A**323** (1992) 611.

[6] R. Blair *et al.* [CDF-II Collaboration],"The CDF-II Detector: Technical Design report," Fermilab-Pub-96/390-E (1996).

[7] T. Zimmerman and M. Sarraj, "A Second Generation Charge Integrator and Encoder ASIC," IEEE NS V433 (June 1996).

[8] The G-LINK transmittter (HDMP-1022) and receiver (HDMP-1024) are described in the Hewlett Packard technical data sheet, "Low Cost Gigabit Rate Transmit/Receive Chip Set with TTL I/Os," http://hsi.web.cern.ch/HSI/components/serialisers/hp/hdmp1022.html.

[9] E. Hazen, J. Rohlf, S. Wu, A. Baden, and T. Grassi, "The CMS HCAL Data Concentrator: A Modular, Standards-Based Implementation," Proceedings of the 7th Workshop on Electronics for LHC Experiments, Stockholm, CERN 2001-005 and CERN/LHCC/2001-034, 347 (2001).

[10] B. G. Taylor, "LHC Machine Timing Distribution for the Experiments," Proceedings of the 6th Workshop on Electronics for LHC Experiments, Krakow (September 2000).

[11] B. G. Taylor, "TTC Distribution for LHC Detectors," IEEE Trans. Nuclear Science, Vol. 45, 821 (1998).

[12] Ph. Farthouat and P. Gallno, RD12 Project Collaboration, "TTC-VMEbus Interface," Version 1.6 (May 2000), http://ttc.web.cern.ch/TTC/intro.html.

[13] P. Gallno, "TTCvx, Technical Description and Users Manual," (May 1999), http://ttc.web.cern.ch/TTC/intro.html.

[14] J. Christiansen, A. Marchioro, P. Moreira, and T. Toifl, RD12 Project Collaboration,"TTCrx Reference Manual," Version 3.4 (December 2001), http://www.pd.infn.it/∼rmartin/dtbx/documents/trigger/ttc_manual.pdf.

[15] The Channel Link is described in the National Semiconductor data sheet, "DS90CR285/DS90CR286, +3.3V Rising Edge Data Strobe LVDS 28-Bit Channel Link-66 MHz," (November 2000), http://www.national.com/parametric/0,1850,1625,00.html.

[16] H.C. van der Bij, O. Boyle, and R. A. McLaren, "S-LINK, a Data Link Interface Specification for the LHC Era", Proceedings of the Beaune 97 Xth IEEE Real Time Conference (1997).

[17] A 64-bit version of S-LINK capable of 800 MBytes per second maximum transfer rate is being developed by the CERN CMS group, http://hsi.web.cern.ch/HSI/s-link.

[18] The Universe II is built by Tundra Semiconductors. The Universe II VME-PCI Bridge device drivers were created by Juergen Hannappel of Bonn University, http://www.llp.fu-berlin.de/pool/software/busses.

[19] The VMEIL also supports the SBS (formerly Bit3) VME-PCI bus adapter, http://www.sbs.com.

[20] Canada-France-Hawaii Telescope, http://software.cfht.hawaii.edu/sspci.

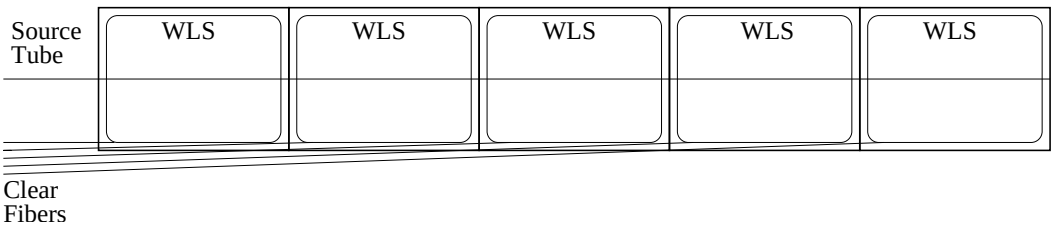

Fig. 1. Portion of a scintillator tray and location of the source tube (not to scale).

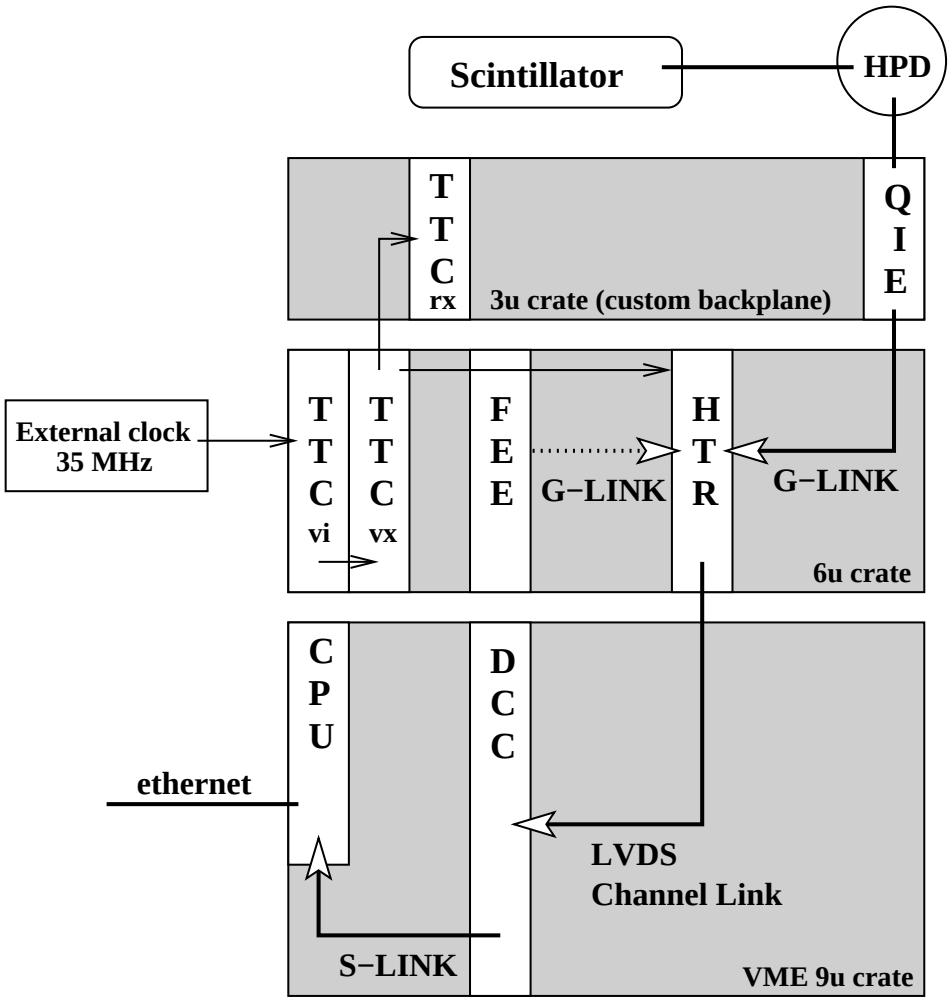

Fig. 2. Block diagram of the apparatus used for the radioactive source measurement. The data path is from the front-end to the HTR by fiber optics (G-LINK), HTR to DCC by twisted pairs (LVDS Channel Link), and DCC to computer by fiber optics (S-LINK).

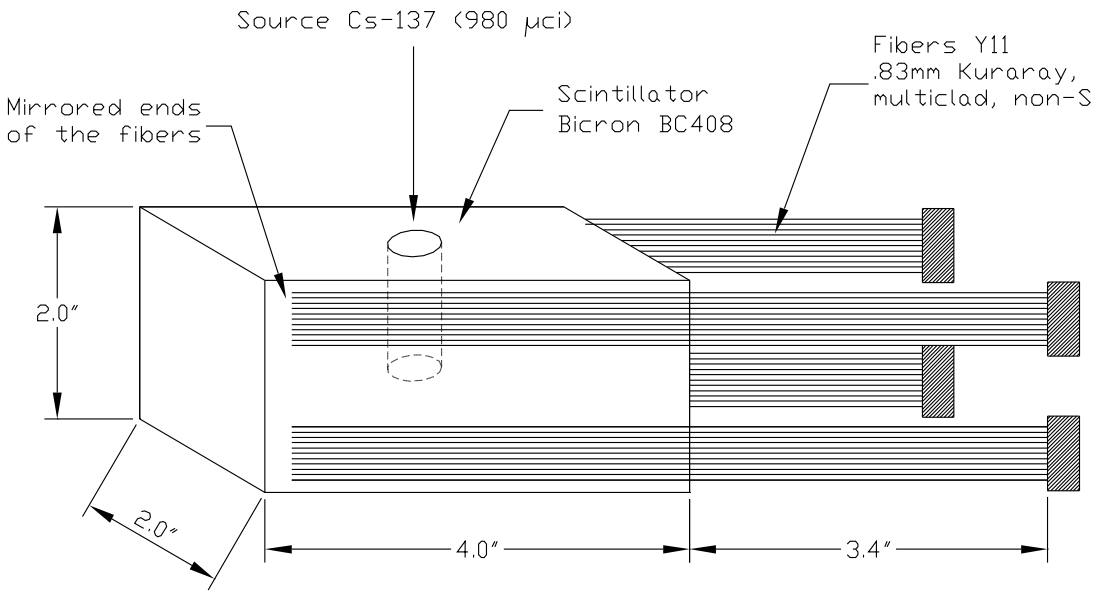

Fig. 3. Geometry of the scintillator used for the radioactive source measurements. Dimensions are in cm,

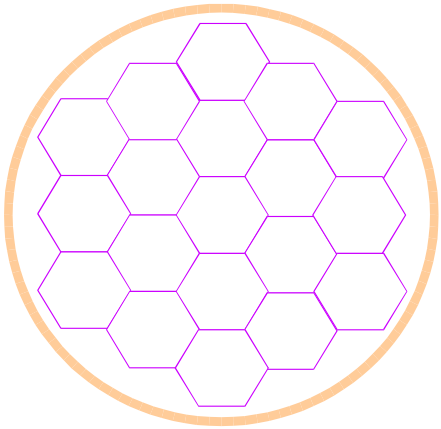

Fig. 4. Pixel arrangement in the hybrid photo-diode.

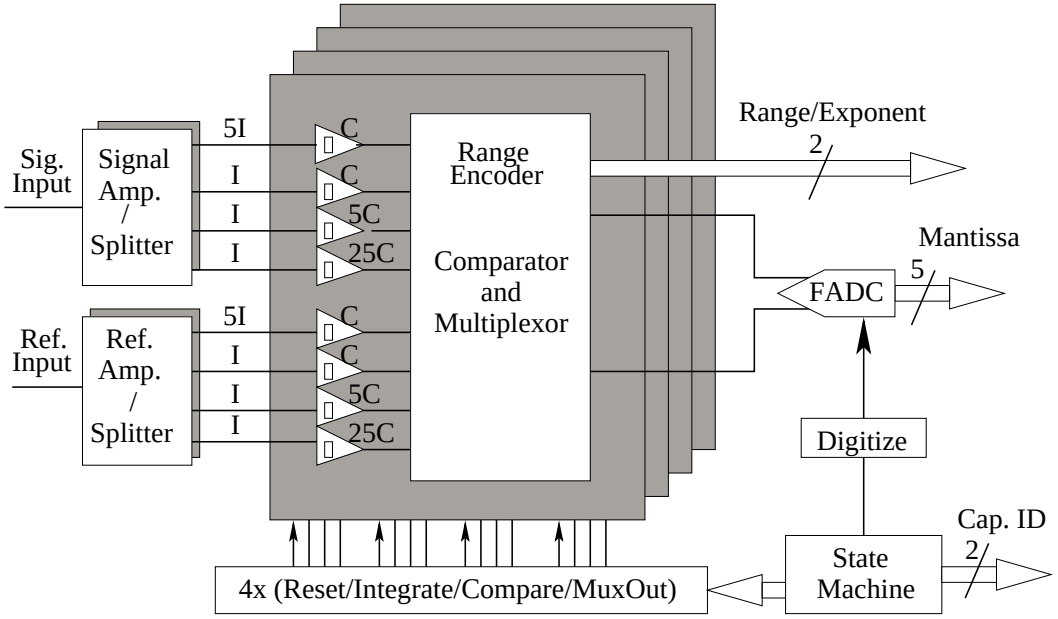

Fig. 5. Block diagram of the QIE8 ASIC.

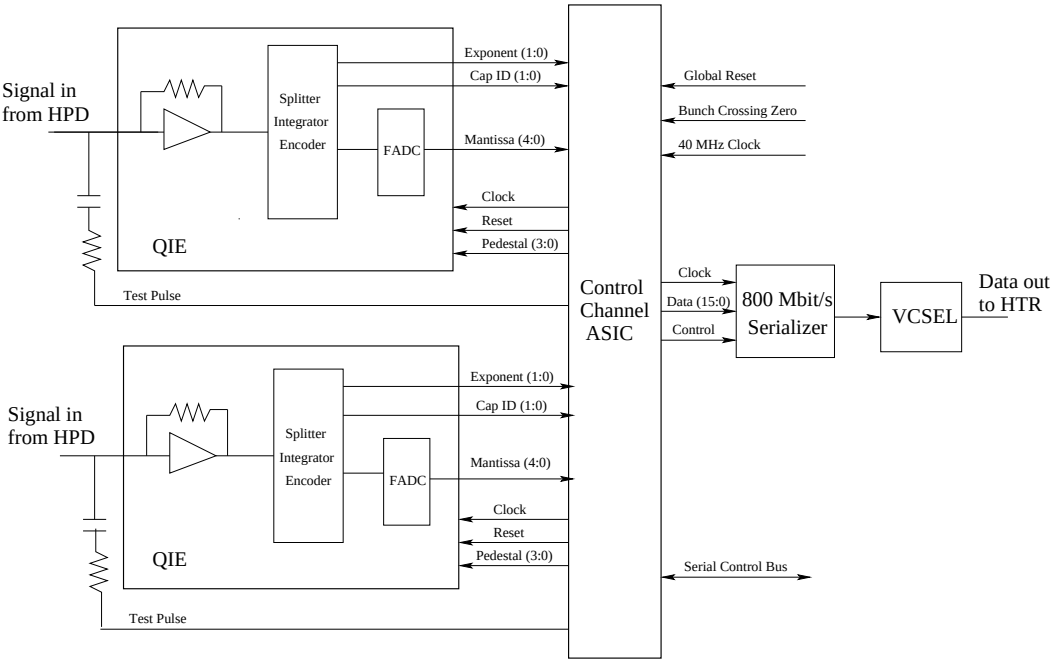

Fig. 6. Block diagram of front-end electronics used for these measurements. Two QIEs feed a control ASIC for transmission on G-Link.

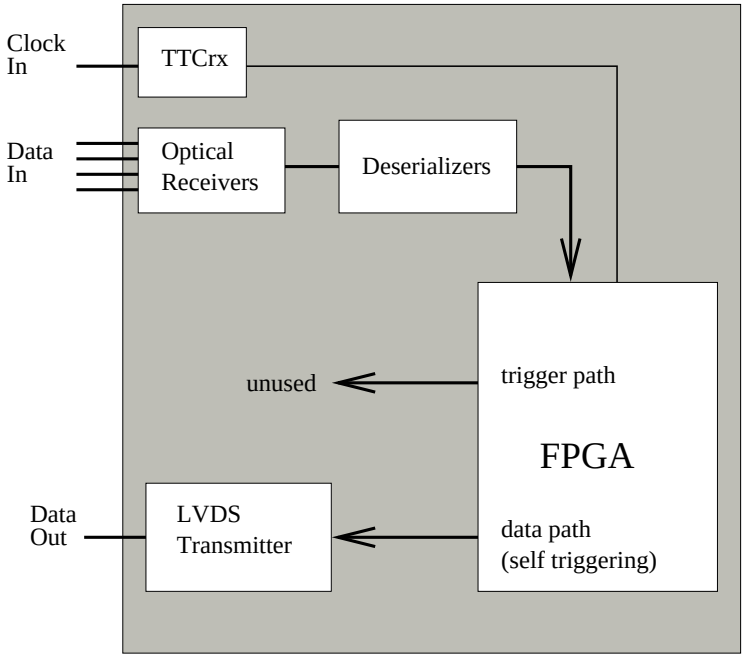

Fig. 7. Block diagram of the prototype HCAL trigger and readout module.

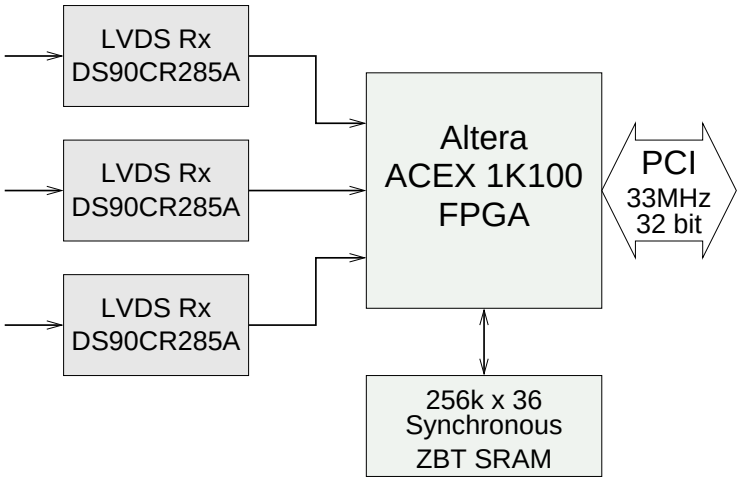

Fig. 8. Block diagram of the LVDS channel link card.

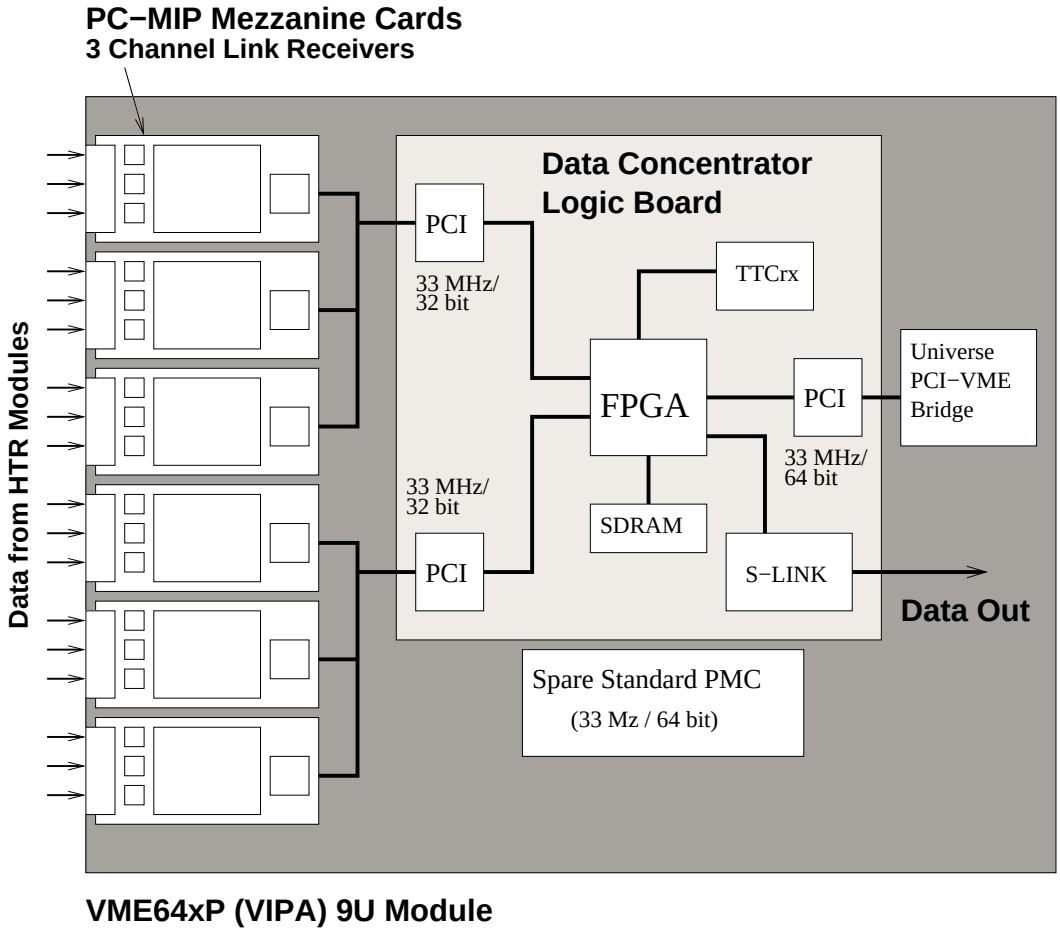

Fig. 9. Architecture of the VME 9u Data Concentrator Card.

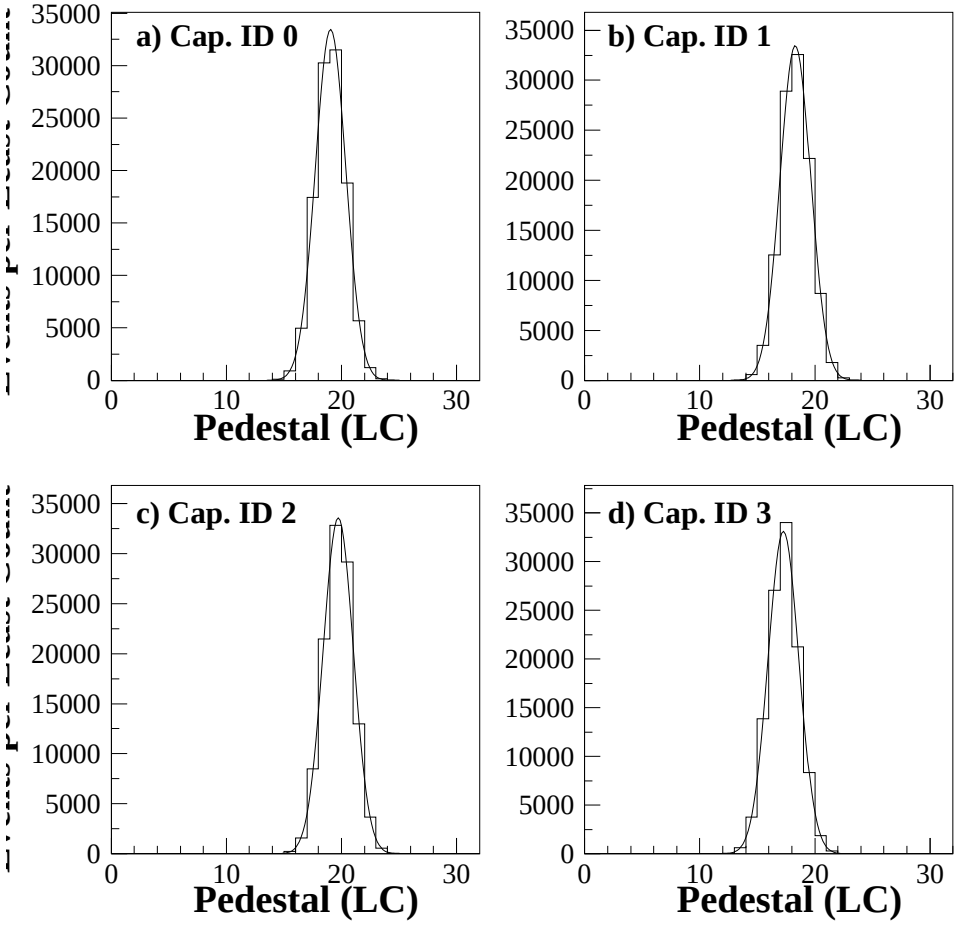

Fig. 10. Pedestal distributions for each of the four capacitors. Each capacitor has a good, but distinct, Gaussian fit.

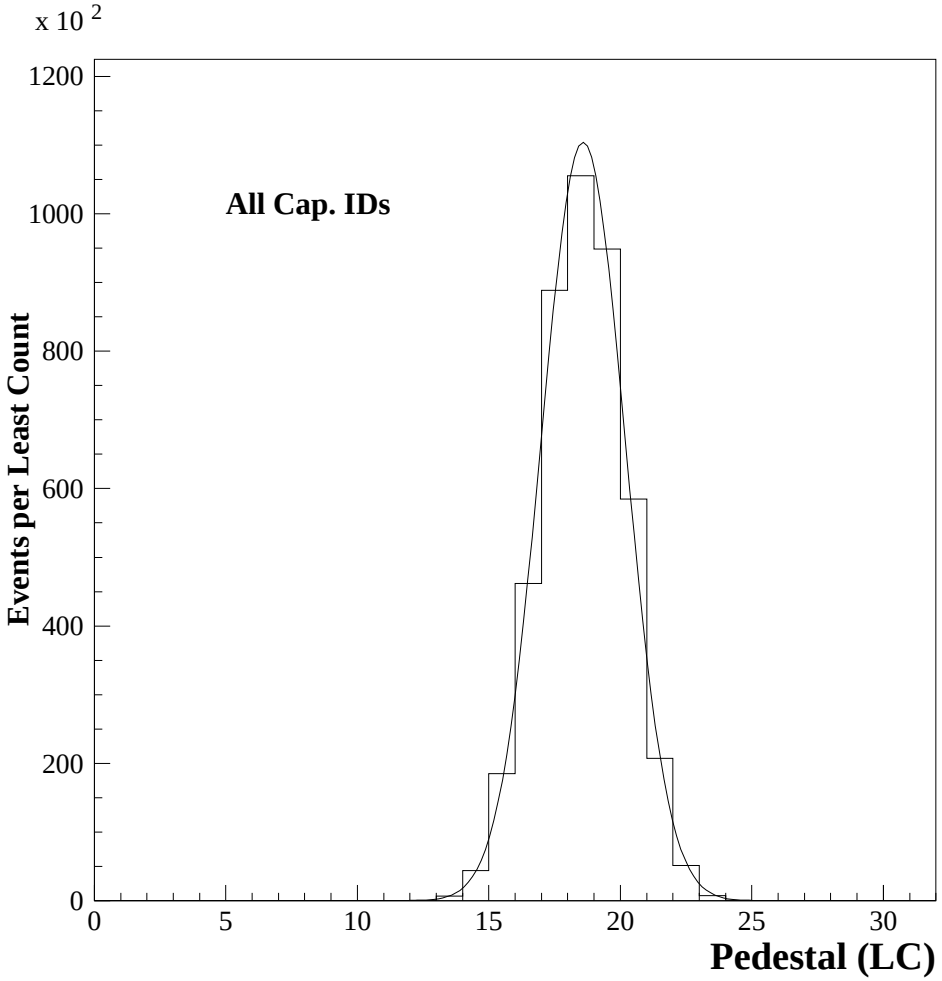

Fig. 11. Pedestal distribution for all four capacitors summed together.

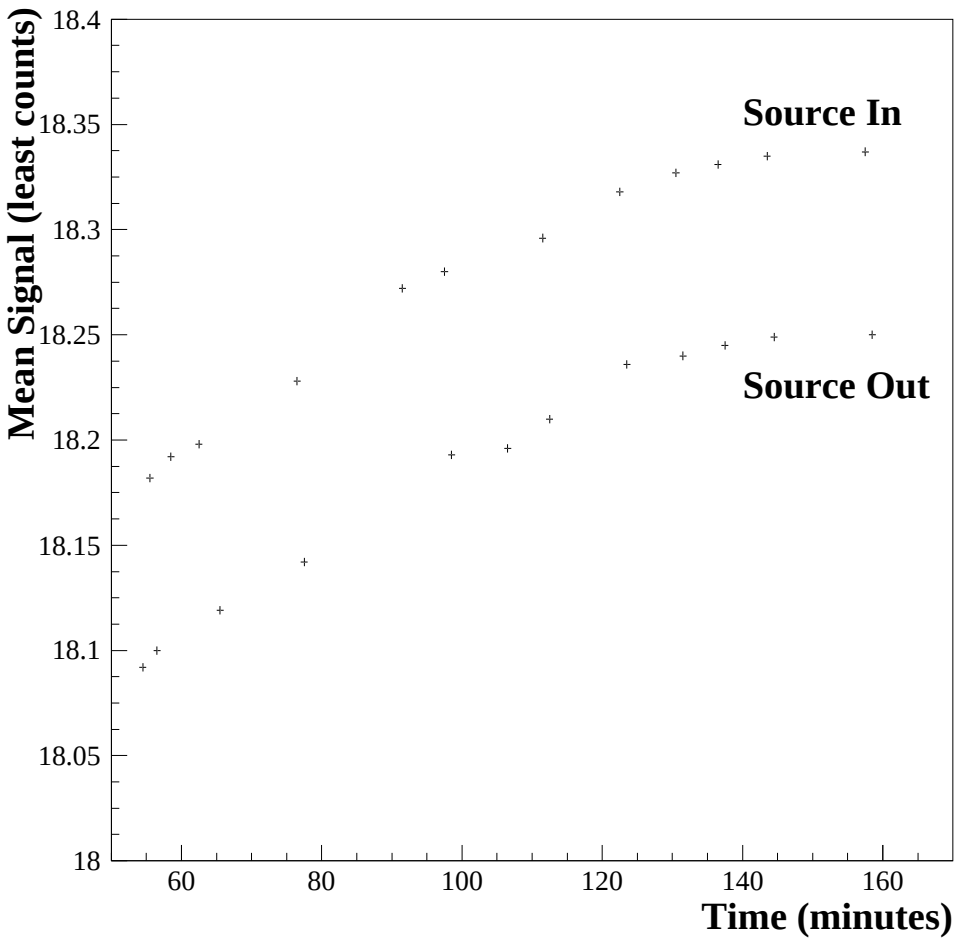

Fig. 12. Plot of mean pedestal and source signal vs. time over a two hour period. The vertical scale has a suppressed zero.

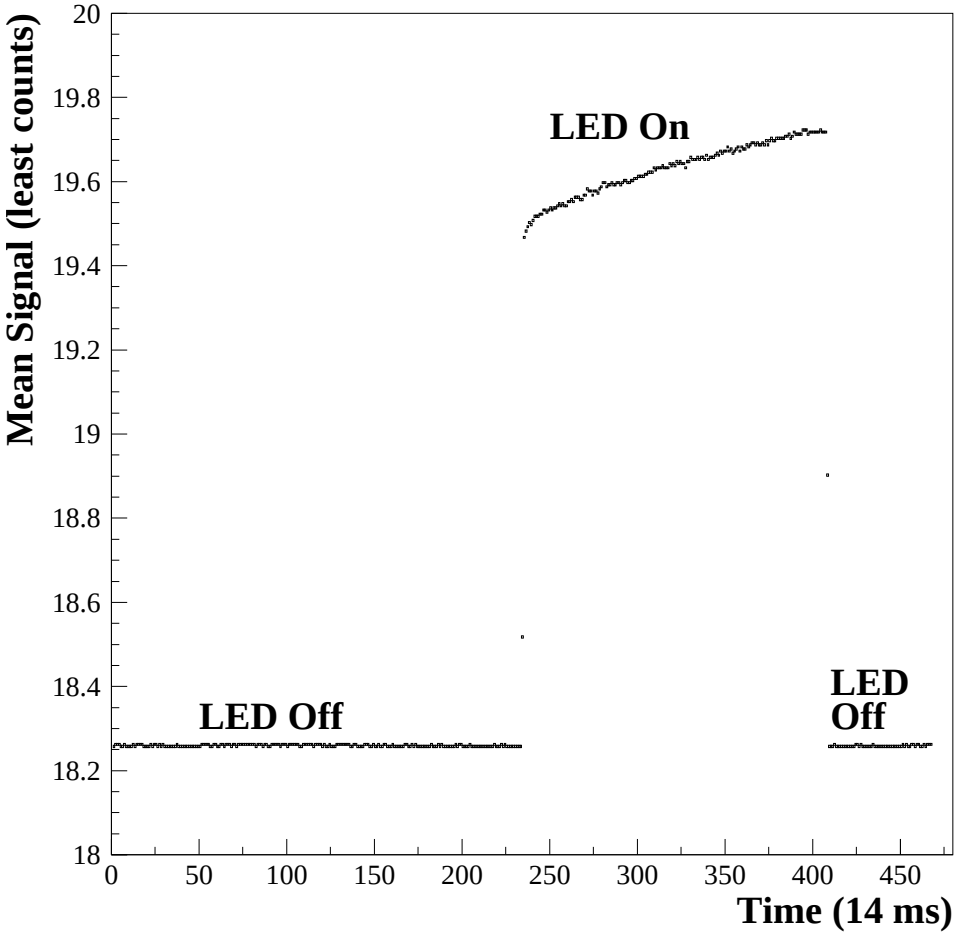

Fig. 13. Plot of the mean signal vs. time as a LED is switched on and then off. Each time bin is 14 ms and the vertical axis is in FADC counts with a suppressed zero.

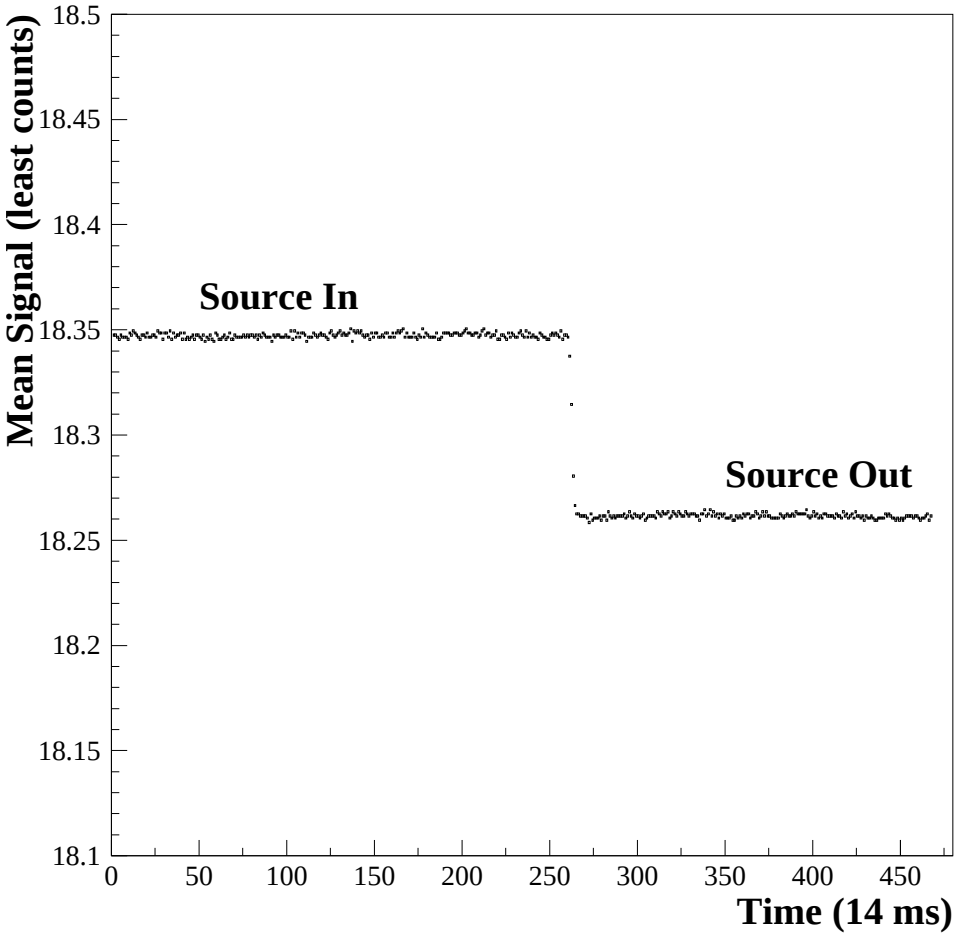

Fig. 14. Plot of the mean signal vs. time as the source is removed. Each time bin is 14 ms and the vertical axis is in FADC counts with a suppressed zero.

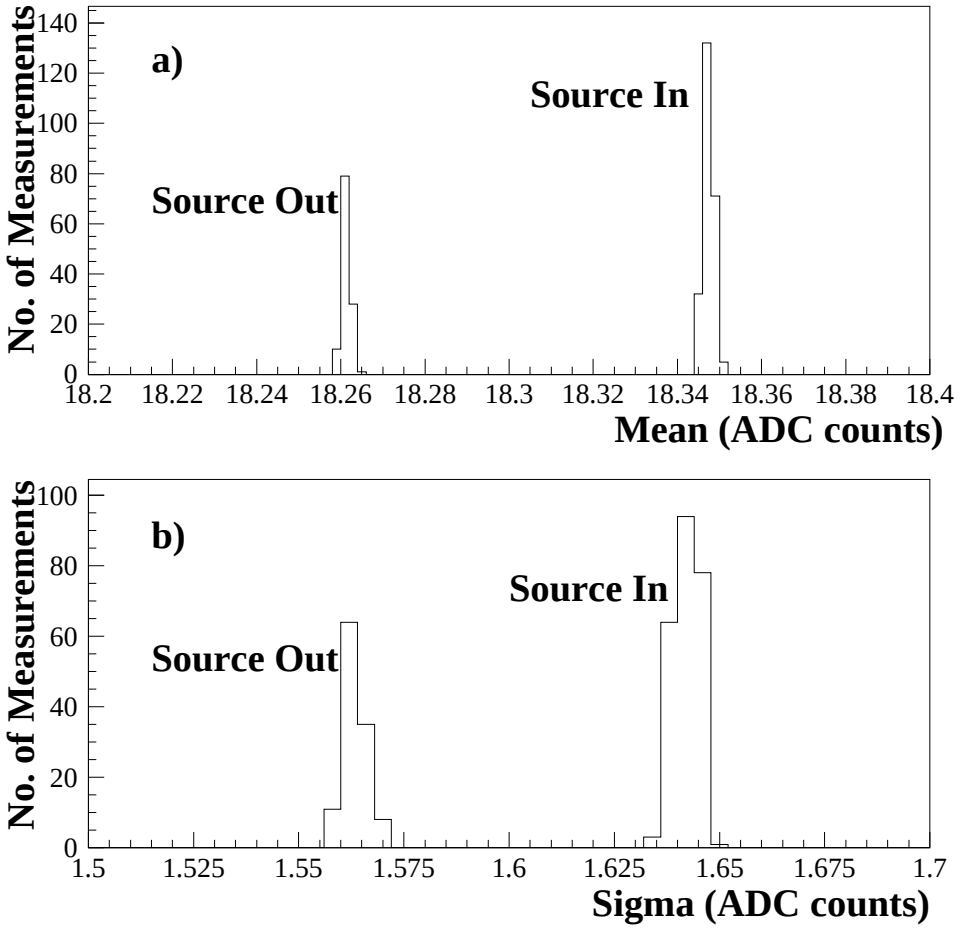

Fig. 15. a) Mean signal for source out and source in, and b) measured sigma for source out and source in.

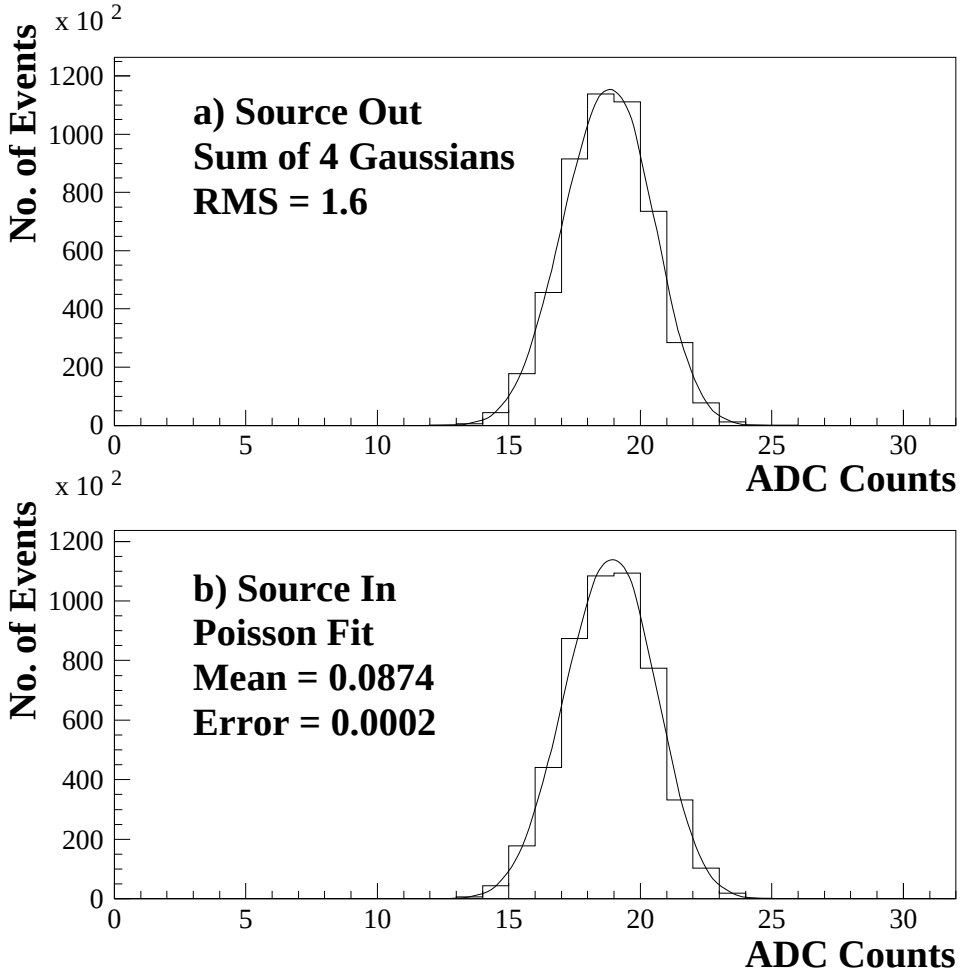

Fig. 16. a) Distribution of 0.5 M events with source out (pedestal). The solid curve is a sum of 4 Gaussian fits to individual cap IDs. b) Distribution of 0.5 M events with source in. The solid curve is a fit to a Poisson distribution added to the pedestal distributions input as fixed parameters.

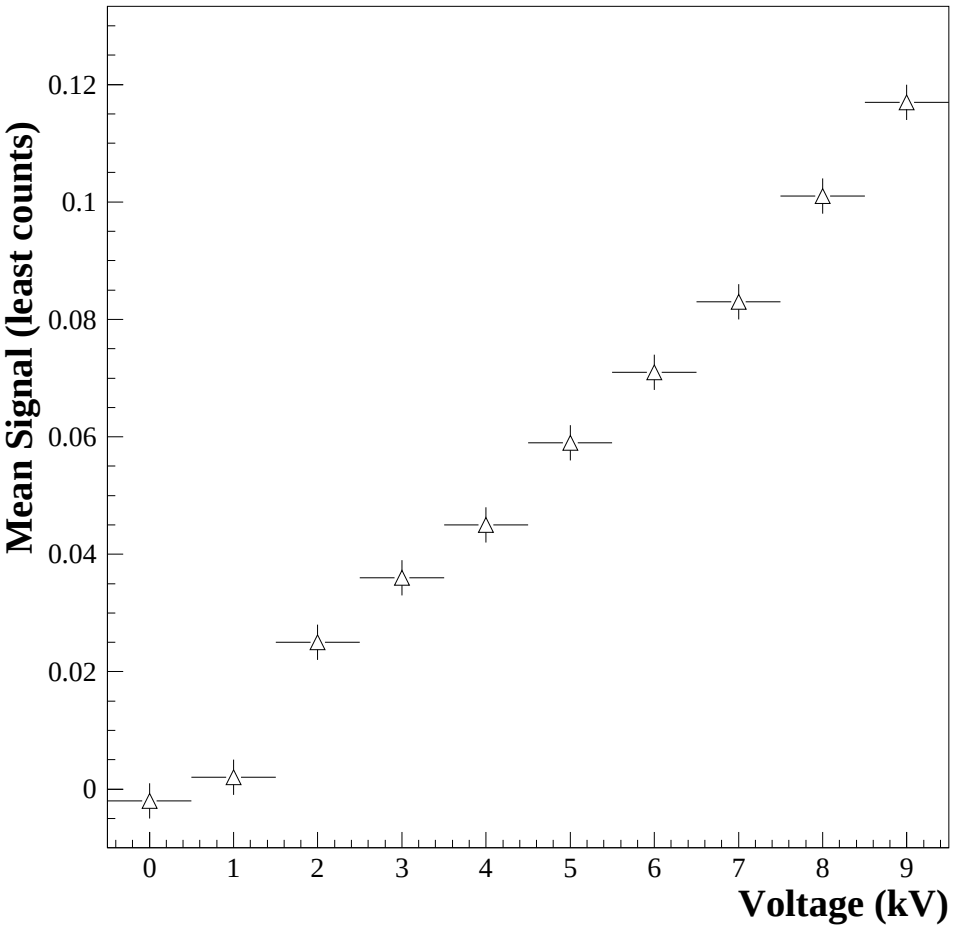

Fig. 17. Mean signal from the radioactive source vs. HPD high voltage.

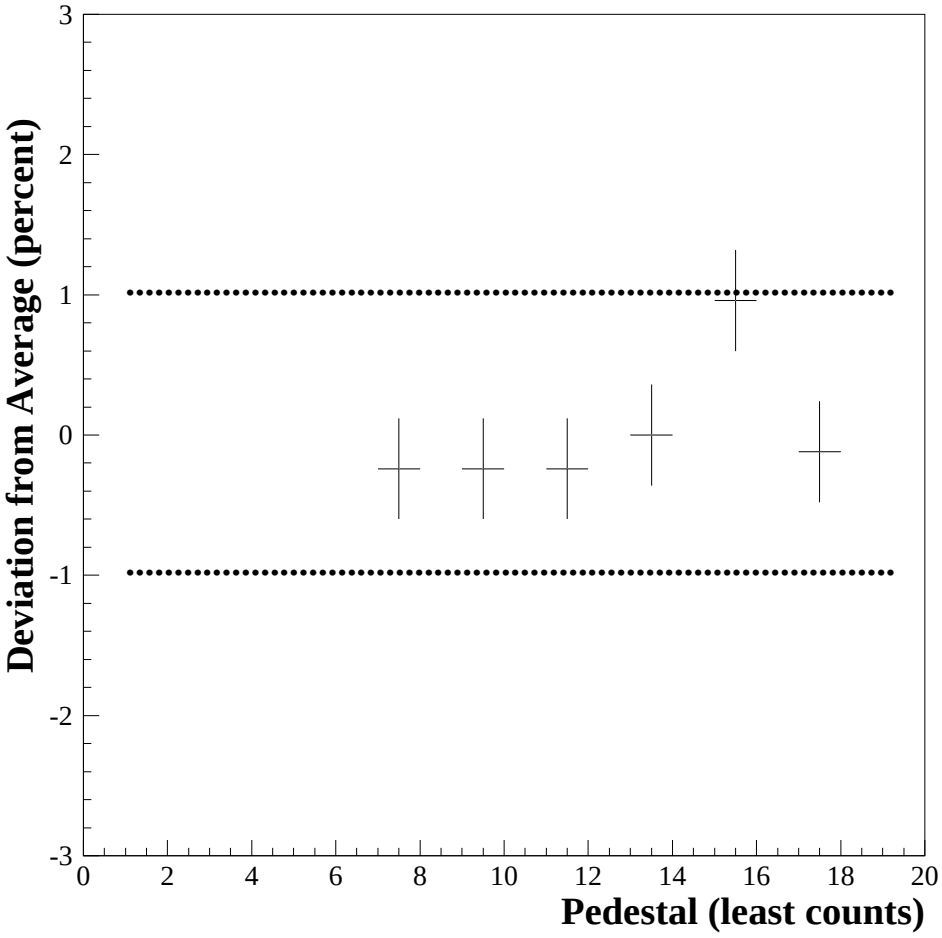

Fig. 18. Contribution of the differential nonlinearity of the QIE. The band indicates a $\pm 1\%$ uncertainty.

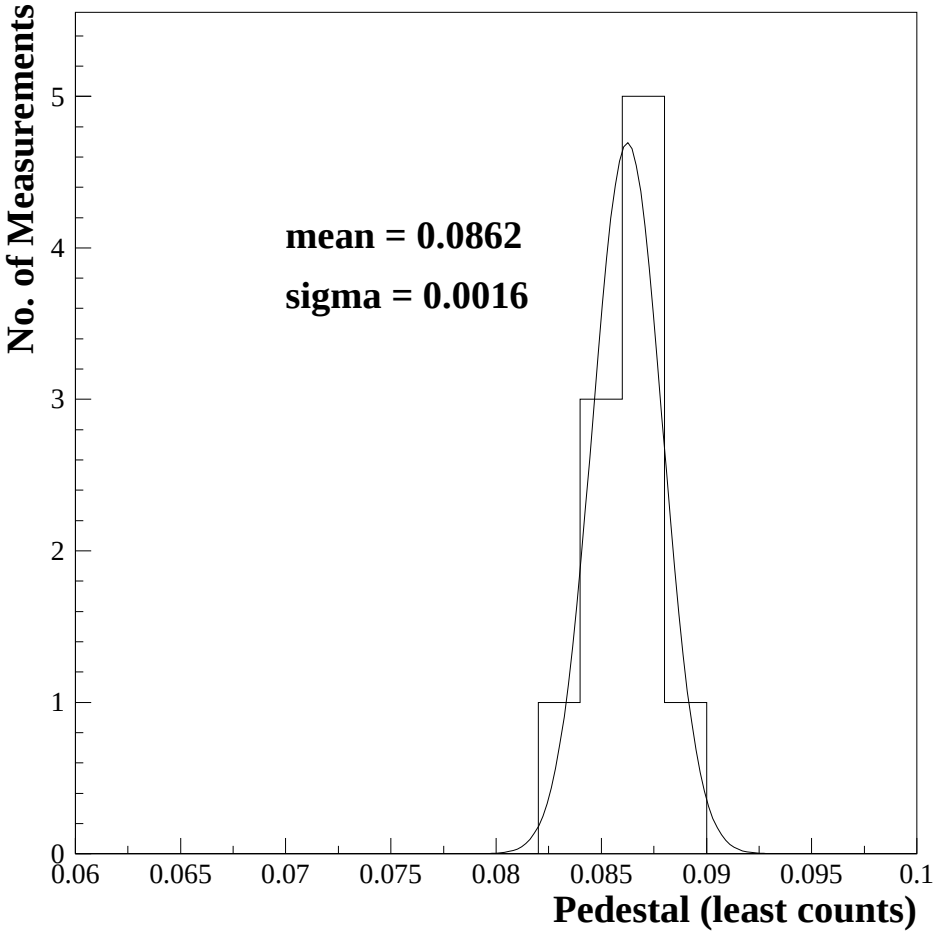

Fig. 19. Distribution of source signals observed over a one month period. The curve is a Gaussian fit.

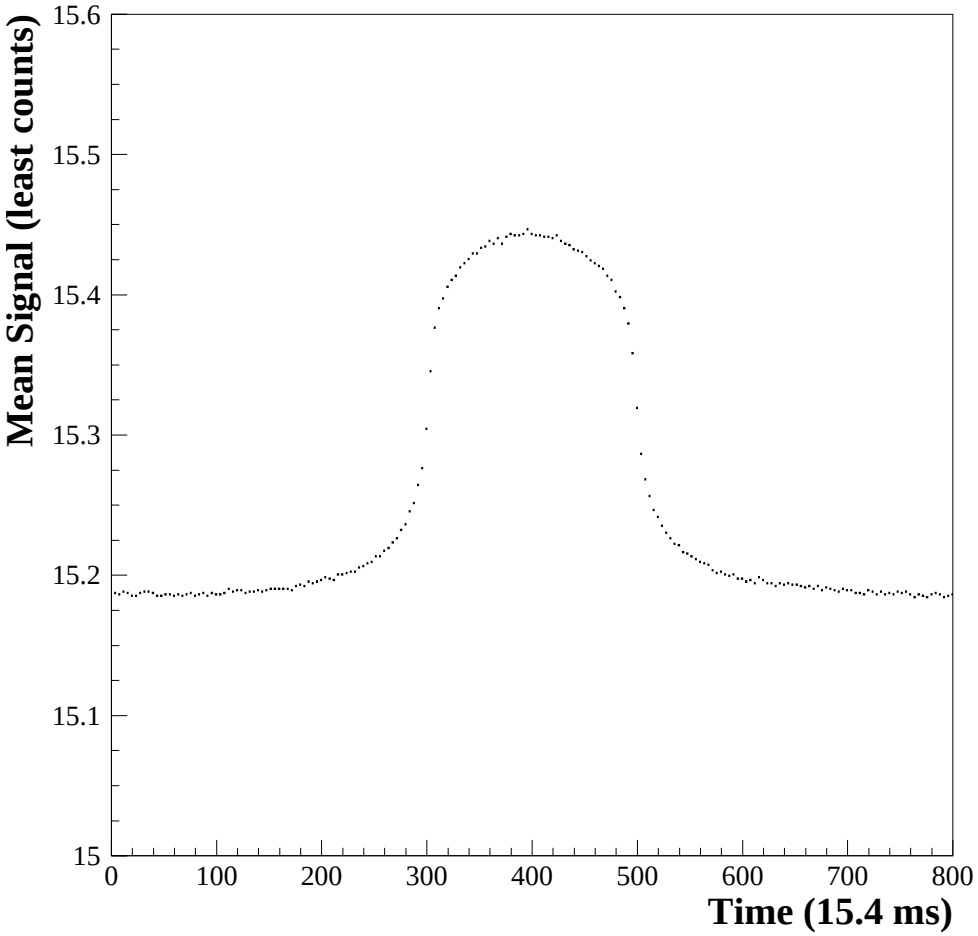

Fig. 20. Source signal observed in the test beam at CERN. Each time bin is 15.4 ms and the vertical axis is in FADC counts with a suppressed zero.The pedestal is measured before and after the source passes over the scintillating tile, which has a width of about 20 cm.